

# Helices and Sheets *in vacuo*†

Martin F. Jarrold

Received 1st September 2006, Accepted 8th December 2006

First published as an Advance Article on the web 19th January 2007

DOI: 10.1039/b612615d

The structures and properties of unsolvated peptides large enough to possess secondary structure have been examined by experiments and simulations. Some of the factors that stabilize unsolvated helices and sheets have been identified. The charge, in particular, plays a critical role in stabilizing  $\alpha$ -helices and destabilizing  $\beta$ -sheets. Some helices are much more stable in vacuum than in aqueous solution. Factors like helix propensity, context, and the incorporation of specific stabilizing interactions have been examined. The helix propensities in vacuum differ from those found in solution. Studies of the hydration of unsolvated peptides can be performed one water molecule at a time. The first few water molecules only bind weakly to unsolvated peptides, and they bind much more strongly to some conformations than to others. The most favorable binding locations are not the protonation sites, but clefts or pockets where a water molecule can establish a network of hydrogen bonds. Non-covalent interactions between secondary structure elements leads to the formation of tertiary structure. Helical peptides assemble into complexes with a variety of intriguing structures. The intramolecular coupling of helices to make antiparallel coiled-coil geometries has also been investigated with model peptides.

## Introduction

While strong covalent bonds link amino acids into linear chains, much weaker non-covalent interactions are responsible for the development of secondary structure, the assembly of tertiary structure domains, the formation of protein assemblies, and the regulatory interactions between proteins. The non-covalent interactions that are important in this arena include both intramolecular interactions and solvent interactions. In nature, the goal is usually not to build the most stable structure or assembly, but to have structures and assemblies that can be regulated or even dismantled in response to the life cycle of the cell or to an external stimulus. For this reason, cellular components are usually marginally stable, and stability is often determined by a delicate balance between solvent and intramolecular interactions. For example, the overall free energy change associated with the folding of a small protein in aqueous solution is relatively small, while there are large changes in both the intramolecular interactions and the solvent interactions. Thus, protein folding is really controlled by a small difference between large numbers. All of the interactions are critical contributors to the overall free energy difference, and so it is difficult to isolate and understand the individual contributions.<sup>1</sup> The ability to separate and study the intramolecular and solvent interactions individually should improve our understanding of these interactions at a fundamental level.

The development of gentle ionization techniques like MALDI and electrospray allow biological molecules to be placed

into the gas phase as anhydrous ions. Under some conditions, the anhydrous ions retain a memory of their solution phase structure.<sup>2,3</sup> Large non-covalent complexes like the chaperonin GroEL (an 800 kDa assembly consisting of 14 proteins) can be transferred into the gas phase intact.<sup>4</sup> These gentle ionization methods permit studies of unsolvated biomolecules. Furthermore, solvent molecules can be added one at a time so that properties can be investigated as a function of the degree of solvation.<sup>5,6</sup> Studies of unsolvated peptides and proteins are of interest for more than just fundamental reasons. Aqueous solution is not the only biologically important environment. Membrane proteins make up to 30% of the proteins encoded by genomes,<sup>7</sup> and the hydrophobic and low dielectric interior of a lipid bilayer is very different from an aqueous environment. The hydrophobic interior of folded proteins is also largely shielded from solvent interactions. So while solvent interactions are obviously important, in many environments the solvent is excluded (or partially excluded). Studies of the intramolecular interactions in the absence of the solvent can help to understand the solvent-depleted regions. A wide variety of techniques have been applied to study unsolvated biomolecules, that range in size from individual amino acids to large protein complexes.<sup>8–25</sup>

This article describes studies of the structures, properties, and hydration of unsolvated peptides with 10–25 residues. This size-regime is larger than has been examined in most gas phase spectroscopic studies,<sup>8–11</sup> and large enough to permit the formation of extended secondary structure elements. In the absence of a solvent, the charge emerges as a critical factor in stabilizing helices and destabilizing sheets. Helices can be much more stable in the gas phase than in solution. In solution, the different amino acids have different propensities to form helices (the helix propensities depend on the side chain). In the gas phase, the ordering of the helix propensities

Chemistry Department, Indiana University 800 East Kirkwood Avenue, Bloomington, 47405, Indiana. E-mail: mffj@indiana.edu  
† The HTML version of this article has been enhanced with colour images.

is changed substantially from in solution. Thus, an amino acid that is a poor helix-former in aqueous solution can be a good helix-former in the absence of a solvent. The role of context (how the specific sequence affects helix stability) and the role of specific stabilizing interactions have been examined. In addition to studies of structure and stability, we have also investigated the hydration properties of model peptides, and found them to be strongly dependent on the conformation. Interactions between helices, which are important in the formation of tertiary structure, have been investigated by studying the assembly of helical complexes and by investigating the formation of an antiparallel coiled-coil geometry in peptides with a designed helix-turn-helix motif.

### Ion mobility measurements

Most of the information described here about the conformations of unsolvated peptide ions was obtained from ion mobility measurements.<sup>26,27</sup> The mobility of a gas phase ion (how rapidly it can be pulled through a buffer gas under the influence of a weak electric field) depends on its average collision cross section, which in turn depends on its structure. Ions with compact, roughly-spherical structures undergo fewer collisions and travel more rapidly than ions with more open, unfolded structures. Geometries are assigned by comparing the measured cross sections to average cross sections calculated for trial geometries, which are usually derived from molecular dynamics simulations.

The experimental apparatus used to perform the majority of the ion mobility measurements is shown schematically in Fig. 1. It consists of an electrospray source, a drift tube, a quadrupole mass spectrometer, and a detector.<sup>28,29</sup> Ions are electrosprayed in air and enter the apparatus through a stainless steel capillary set in a heated copper–beryllium block. The capillary ends in a differentially pumped region that is maintained at 0.2 torr. Some of the ions pass through this region and into the main chamber where they are focused through an electrostatic shutter into a 30.5 cm long drift tube. The drift tube is operated with a helium buffer gas pressure of 2–5 torr, and with a drift field of 5–13 V cm<sup>-1</sup>. Field guard rings along the drift tube ensure that there is a uniform electric field near to the drift tube axis. Under the conditions employed, the drifting ions remain in the low field limit<sup>30</sup> where they are not significantly heated or aligned by the field. After travelling

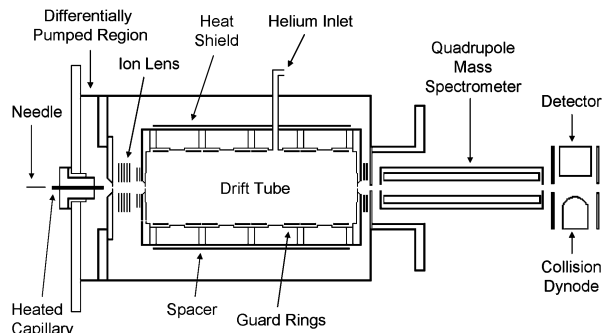


**Fig. 1** Schematic of diagram of the experimental apparatus equipped with the high temperature drift tube. (From ref. 29. © American Chemical Society 2004).

across the drift tube, some of the ions exit through a small aperture. The exiting ions are focused into a quadrupole mass spectrometer where they are mass analyzed, and then detected.

Two drift tubes were employed, a low temperature version (77–400 K) and a high temperature version (300–1100 K). In both cases, the temperature was regulated by microprocessor-based temperature controllers to within  $\pm 1$  K. Drift time distributions (the amount of time it takes ions to travel across the drift tube) are obtained using an electrostatic shutter to admit 50–100  $\mu$ s packets of ions into the drift tube. A multi-channel scaler, synchronized with the shutter, records the arrival time distributions at the detector for mass-selected ions. The drift time distribution is then obtained by correcting the arrival time distribution for the time the ions spend travelling outside the drift tube. Drift times are converted into cross sections using standard methods.

The peptides were synthesized using *FastMoc* chemistry on an Applied Biosystems 433A peptide synthesizer. After synthesis, they were cleaved, precipitated, and lyophilized. Most of the peptides were acetylated at the N-terminus prior to deprotection of the basic side chains. Electrospray solutions were prepared by dissolving 1 mg of the unpurified peptide in 1 mL of TFA and 0.1 mL of purified water.

### Molecular dynamics simulations

Molecular Dynamics (MD) simulations were performed to help interpret the experimental results. The simulations were done with the MACSIMUS suite of programs<sup>31</sup> using the CHARMM21.3 parameter set. A dielectric constant of 1.0 was employed. Average cross sections for structures derived from the MD simulations were calculated with MOBCAL,<sup>32</sup> which accounts for multiple scattering events<sup>33</sup> and the long-range interactions between the ion and the buffer gas.<sup>34</sup> If the geometry from the simulations is correct, the measured and calculated cross sections are expected to agree to within  $\pm 2\%$ .

The objective of the MD simulations is to locate the low energy conformations. A variety of starting structures were employed (such as helix, sheet, and extended linear chain) and a number of simulated annealing schedules were used in an effort to escape high energy local minima. Often, hundreds of simulations were performed to explore the energy landscape of a particular peptide. In some cases, MD with simulated annealing was unable to locate the lowest energy conformation and more sophisticated methods were used (see description of evolutionary based methods below). Ion mobility measurements are not particularly sensitive to structural details. However, since these studies deal with relatively large peptides, we are more concerned with identifying structural types than in their fine details. In addition, at room temperature the structures are expected to show fluctuations and so the average structure is more relevant than the lowest energy conformation. In some cases, the average room temperature structure is significantly different from the lowest energy conformation.

### Design of unsolvated helices

Fig. 2 shows examples of ion mobility measurements for protonated AcA<sub>15</sub>K and AcKA<sub>15</sub> (Ac = acetylated, K =

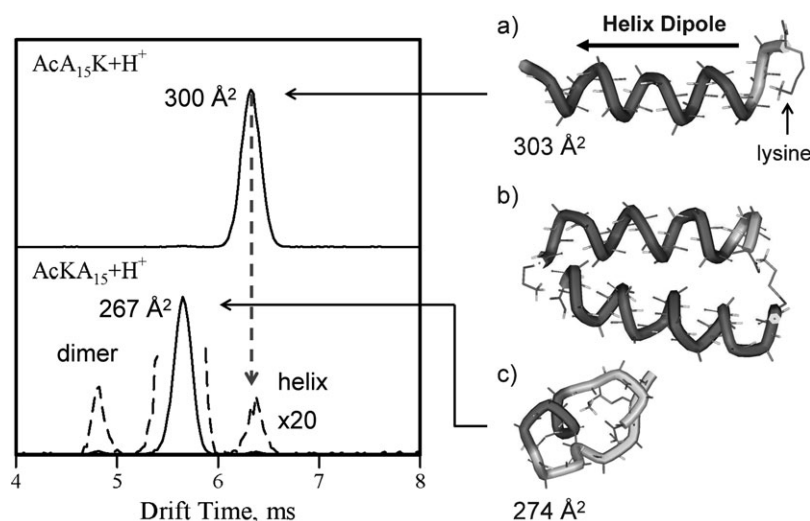


**Fig. 2** Drift time distributions measured for protonated AcA<sub>15</sub>K and AcKA<sub>15</sub>. The structures on the right are snap shots taken from MD simulations. (a) is an AcA<sub>15</sub>K + H<sup>+</sup> helix; (b) is an AcKA<sub>15</sub> + H<sup>+</sup> helical dimer, and; (c) is an AcKA<sub>15</sub> + H<sup>+</sup> globule.

lysine, A = alanine). Since the N-terminus is acetylated in these peptides, the most favorable protonation site is the lysine side chain. For AcA<sub>15</sub>K + H<sup>+</sup> there is a single peak in the drift time distribution corresponding to a cross section of 300 Å<sup>2</sup>. The average cross section calculated for the helical conformation of AcA<sub>15</sub>K + H<sup>+</sup> from MD simulations is 303 Å<sup>2</sup>. AcA<sub>15</sub>K was designed to be helical:<sup>35,36</sup> alanine has a high helix propensity in solution.<sup>37–39</sup> In addition, protonation at the C-terminus lysine stabilizes the helix through favorable interactions with the helix macrodipole<sup>40–42</sup> and through helix capping interactions.<sup>43,44</sup> In an ideal  $\alpha$ -helix, the four residues at each end of the helix lack hydrogen bonding partners. In AcA<sub>15</sub>K + H<sup>+</sup>, the protonated  $\epsilon$ -amino group of lysine caps the helix by forming hydrogen bonds to the dangling carbonyl groups at the C-terminus. The NH–CO peptide bond group has a significant dipole moment (around 3.5 D) and alignment of the dipoles along the length of the helix leads to a macrodipole. The negative end of the macrodipole is at the C-terminus, and so a positive charge at the C-terminus stabilizes the helix, and a positive charge at the N-terminus destabilizes the helical conformation. AcKA<sub>15</sub> + H<sup>+</sup>, where the charge destabilizes the helix, adopts a globular conformation.

### The globule

The globule is a compact, random-looking, three-dimensional structure. An example is shown in Fig. 2(c). The main organizing criteria for the globule appears to be maximizing self-solvation of the charge (the backbone CO groups point at, and coordinate to, the –NH<sub>3</sub><sup>+</sup> group) and maximizing the number of non-covalent interactions, both of which are realized by achieving a compact, near-spherical arrangement. There are many possible globular conformations. The average cross section for the lowest energy globule found for AcKA<sub>15</sub> + H<sup>+</sup> in the MD simulations is significantly (> 2%) larger than the measured value. We attribute this deviation to the difficulty in finding compact, low energy globular conformations. Both MD and Monte Carlo appear unable to locate low

energy globular conformations with cross sections that match the experimental values. Raising the temperature to promote transitions out of local minima tends to drive the structure towards more open conformations, so simulated annealing has also had limited success at finding compact globules. Compact, low energy globular conformations with cross sections that match the experimental values have, however, been located by an evolutionary-based method.<sup>45</sup> Evolutionary methods of structural optimization operate on a pool of geometries and incorporate recombination (mating) and mutations to explore the energy landscape. The particular application employed here (FOLDAWAY) also optimized the progeny prior to evaluating their energy.

### Helical dimers

In addition to the globule, there are two other conformations present (at low relative abundance) in the drift time distribution for AcKA<sub>15</sub> + H<sup>+</sup>. The one at shorter time (around 4.8 ms) is attributed to a helical dimer. A snap-shot of the helical dimer conformation is shown in Fig. 2(b). It consists of two AcKA<sub>15</sub> + H<sup>+</sup> helices aligned head-to-toe with the protonated lysine side chain of one peptide interacting with the C-terminus of the other. This “exchanged-lysine” arrangement allows the AcKA<sub>15</sub> + H<sup>+</sup> peptides to adopt helical conformations (the AcKA<sub>15</sub> + H<sup>+</sup> monomer is a globule because protonation at the N-terminus lysine destabilizes the helix). When observed directly from solution, AcKA<sub>*n*</sub> + H<sup>+</sup> with *n* > 13 is predominantly in the helical dimer form, while *n* < 13 is predominantly in the monomeric globular form. The monomeric globule present in the drift time distribution for AcKA<sub>15</sub> + H<sup>+</sup> in Fig. 2 results from dissociation of the dimer. As the ions enter the drift tube their kinetic energy is thermalized by collisions with the buffer gas. During this process they undergo a transient heating cycle where their internal energy is initially increased, and then thermalized, after the ions are stopped by the buffer gas. If the structures coming from solution are significantly different from the lowest-free-energy gas-phase

structure, the ions may undergo a conformational change while they are hot. So this transient heating cycle provides a way to investigate how the gas phase structures differ from the solution phase. In the present case, dimers that are present in solution (or form during the electrospray process) dissociate when they are collisionally heated. If the injection energy into the drift tube is decreased, the amount of helical dimer present in the drift time distribution increases. In addition to the helical dimer and monomeric globule, the drift time distribution for  $\text{AcKA}_{15} + \text{H}^+$  (Fig. 2) shows a small peak at a drift time corresponding to the helix. This small amount of  $\text{AcKA}_{15} + \text{H}^+$  helix is believed to result from a dimer dissociation process, where the proton transfers from the lysine side chain to the C-terminus of the helical peptide.

### The high temperature stability of some unsolvated helices

Isolated  $\alpha$ -helices are only marginally stable in solution. Even designed alanine-based peptides (which are among the most strongly helical peptides in aqueous solution) consist of an ensemble of partially helical structures that are on average only around 50% helical at room temperature, and almost completely melted at 70 °C.<sup>46,47</sup> In contrast, unsolvated  $\text{AcA}_{15}\text{K} + \text{H}^+$  remains essentially 100% helical up to at least 425 °C (700 K).<sup>48</sup> Fig. 3 shows measured and calculated cross sections for the  $\text{AcA}_{15}\text{K} + \text{H}^+$  helix and  $\text{AcKA}_{15} + \text{H}^+$  globule as a function of temperature. The open points are the experimental results. The filled points are Boltzmann-weighted average cross sections from MD simulations performed as a function of temperature. The lines in Fig. 3 result from taking the lowest energy conformation from the room temperature MD simulations and calculating the cross section for this

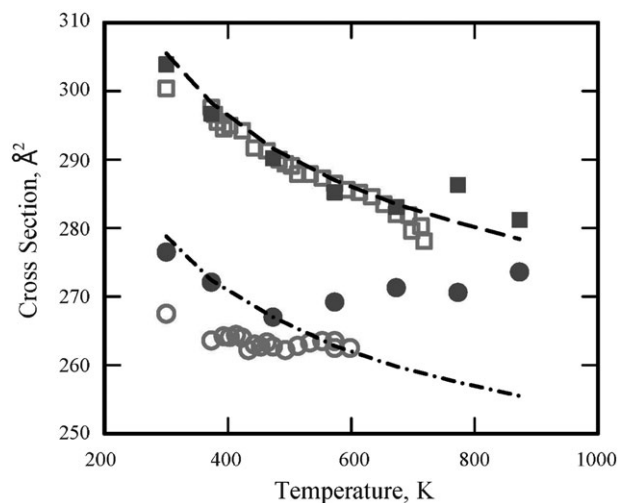


**Fig. 3** Measured and calculated cross sections for the  $\text{AcA}_{15}\text{K} + \text{H}^+$  helix and  $\text{AcKA}_{15} + \text{H}^+$  globule as a function of temperature. The open points are the measured values for  $\text{AcA}_{15}\text{K} + \text{H}^+$  (squares) and  $\text{AcKA}_{15} + \text{H}^+$  (circles). The filled points are Boltzmann weighted average cross sections from MD simulations performed as a function of temperature. The lines result from taking the lowest energy conformation from the room temperature MD simulations and calculating cross sections for this structure as a function of temperature,  $\text{AcA}_{15}\text{K} + \text{H}^+$  (dashed line) and  $\text{AcKA}_{15} + \text{H}^+$  (dashed-dotted line). (From ref. 48. © American Chemical Society 2004).

structure as a function of temperature. This shows the cross sections that would result, as a function of temperature, for rigid helical and globular conformations. The cross sections for the rigid conformations systematically decrease. This occurs because the long range interactions between the ion and the buffer gas atoms become less important as the temperature is raised. When the measured cross sections (or the Boltzmann-weighted average cross sections) deviate significantly from the cross sections calculated for the rigid conformations, it indicates a conformational change. For the  $\text{AcA}_{15}\text{K} + \text{H}^+$  helix, the experimental results and the Boltzmann-weighted average cross sections remain in good agreement up to around 700 K, indicating that the peptide remains in the rigid helical conformation up to this temperature. At about 725 K, the signal for the helix disappears due to fragmentation. Thus, the  $\text{AcA}_{15}\text{K} + \text{H}^+$  peptide remains helical all the way up to the point where it fragments. The high stability of the unsolvated helices is consistent with simulations.<sup>49–51</sup> In MD simulations performed at 673 K, the  $\text{AcA}_{15}\text{K} + \text{H}^+$  helix remains largely intact, however at 773 K the structure fluctuates between helix, globular, and unfolded (random coil-like) conformations and the Boltzmann-weighted average cross section deviates significantly from the cross section for the rigid helix. Note that we can perform MD simulations above the temperature where the peptide fragments because the force field does not permit covalent bond breaking. In the simulations, helix melting is usually initiated by fraying at the N-terminus (*i.e.*, away from the charge). In the reverse process, forming the helix from a random structure, the protonated lysine side chain plays a critical role in nucleating the helix. In the simulations, the protonated amino group acts as a template, and then caps the first turn of the helix. The helix then propagates from both ends to form a completely helical conformation. The idea of a remote helix nucleator (as the lysine is behaving here) is not incorporated into the statistical-mechanical models of helix formation, such as the models of Zimm and Bragg<sup>52</sup> and Lifson and Roig,<sup>53</sup> and their more recent refinements.<sup>54–58</sup> The basic idea behind these models is that there is a nucleation step that is associated with fixing a few neighboring residues into a helical conformation so that the first helical hydrogen bond can be made, and then follows a propagation phase where residues add onto the end of the growing helix, each one making a new helix hydrogen bond. There is an entropic penalty for fixing the first few residues, while helix propagation has a favorable free energy change. In unsolvated  $\text{AcA}_{15}\text{K} + \text{H}^+$ , the lysine side chain helps to overcome the penalty for helix nucleation by templating and capping the nascent helix. This may explain why the application of the statistical-mechanical models to helix formation in unsolvated peptides met with limited success.<sup>59</sup>

### Mobile protons

Protonated polyalanine peptide ions,  $\text{A}_n + \text{H}^+$ , lack a residue with a basic side chain. The most likely protonation sites are the N-terminus amine and the backbone amide CO groups.<sup>60–63</sup> According to MD simulations, the globule is the lowest energy conformation when protonated at the

N-terminus amine, but when the proton is on the amide CO nearest the C-terminus the helix has the lowest energy, at least for peptides with 10–25 residues. The acetylated analogs of these peptides (where the N-terminus amine is blocked) are 100% helical. This indicates that when the N-terminus is blocked the proton is sequestered at the C-terminus.

Initial studies suggested that  $A_n + H^+$  peptides adopt globular conformations in the gas phase.<sup>64</sup> However, it now seems that this reflected the preferred solution phase conformation, because when the peptide ions are collisionally heated as they enter the drift tube both the helix and globule are observed. Thus, the energies of the helix and globule are quite similar for unsolvated  $A_n + H^+$  peptides, and interconversion between these conformations is possible. This interconversion must involve proton transfer from one end of the peptide to the other. Intramolecular proton transfer in ionized peptides has received a lot of attention in connection with peptide fragmentation patterns obtained by mass spectrometry.<sup>65–68</sup> In order to account for the observed fragmentation patterns, it is necessary to assume that the proton is not sequestered at the most basic sites, but that it is free to migrate before dissociation occurs (*i.e.*, a mobile proton). Fig. 4 shows drift time distributions recorded for  $A_{20} + H^+$  as a function of tem-

perature. At 373 K there are two peaks present due to the globule (short drift time) and helix. As the temperature is raised the distribution remains unchanged up to around 413 K, where the gap between the two peaks starts to fill-in. This indicates that the ions are beginning to undergo conformational changes on the time scale of the drift time measurements. Ions that fill-in the region between the two peaks spend part of their time travelling through the drift tube in one conformation, and part of their time in the other. As the temperature is raised, interconversion between the helical and globular conformations becomes more rapid, and the region between the two peaks becomes more populated. Eventually, interconversion becomes fast compared to the time spent travelling across the drift tube, and the broad feature narrows. The position of the narrow peak relative to the expected position of the helix and globule informs on the amount of time spent in each conformation at high temperature. In the present case, the peak at 473 K is closer to the expected position of the helix than the globule, indicating that, at high temperature,  $A_{20} + H^+$  spends most of its time in a helical conformation.  $A_{15} + H^+$ , on the other hand, spends most of its time in the globular conformation. Since interconversion between the helix and globule requires proton transfer from one end of the peptide to the other, the onset of interconversion (between 400 and 450 K) indicates the temperature where the proton becomes mobile in these peptides.

#### $\beta$ -sheets and helices in the absence of a charge

Our efforts to observe a stable, unsolvated  $\beta$ -sheet structure for charged peptides were unsuccessful. According to simulations, the charge disrupts extended  $\beta$ -hairpins and other  $\beta$ -structures by causing the peptide to wrap up around the charge site. There have been some suggestions of  $\beta$ -structures for charged peptides in the gas phase,<sup>69,70</sup> but these are usually short sections, and there is no compelling evidence for an extended  $\beta$ -structure in an unsolvated peptide when a charge is present.

Since a charge can stabilize a helix in an unsolvated peptide, and it apparently destabilizes  $\beta$ -structures, what conformations are favored in the absence of a charge? Electric deflection measurements have been used to investigate the conformations of neutral peptides.<sup>71,72,73</sup> The total dipole moment of a peptide is mainly due to the dipole moments of the NH–CO peptide bond group (which is around 3.5 D). For  $\alpha$ -helices, the dipoles are aligned leading to a very large overall dipole moment. For a  $\beta$ -sheet, the dipoles almost cancel and the overall dipole moment is small. For a globular conformation on the other hand, the dipoles are expected to be randomly orientated with respect to each other, leading to an overall dipole moment that is larger than a  $\beta$ -sheet, but substantially less than for a helix. Thus, the overall dipole moment can be used to deduce the conformation.

Dipole moments were obtained from electric deflection measurements that were performed in collaboration with Dr Philippe Dugourd and his group at the Laboratoire de Spectrométrie Ionique et Moléculaire at Université Lyon. The measurements were performed on an apparatus consisting of a matrix-assisted laser-desorption source coupled to a

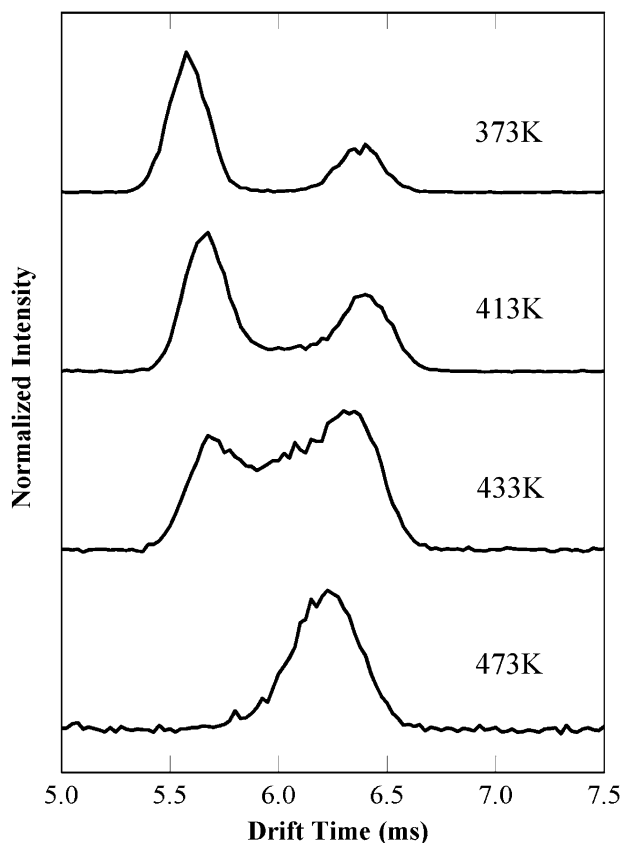


**Fig. 4** Drift time distributions recorded for  $A_{20} + H^+$  as a function of temperature. The larger peak on the left at 373 K is due to the globule while the smaller peak on the right is due to the helix. When the temperature is raised the helix and globule interconvert. The position of the peak at high temperature indicates that the peptide spends most of its time in a helical conformation. (From ref. 29. © American Chemical Society 2004).

molecular beam deflection apparatus with a position-sensitive time-of-flight mass spectrometer.<sup>74,75</sup> The peptides are desorbed with a pulsed Nd:YAG laser (355 nm), entrained in a pulsed helium flow, and thermalized in a 5 cm long diverging nozzle. After leaving the nozzle, the beam is tightly collimated before it travels through the 15 cm long electric deflector. The deflector provides an electric field  $F$  and a field gradient  $(\partial F/\partial z)$  perpendicular to the beam axis. One meter after the deflector, the molecular beam is irradiated with the fourth harmonic of a Nd:YAG laser (266 nm) in the extraction region of the position sensitive time-of-flight mass spectrometer. The peptides studied using this approach incorporate a tryptophan (W) residue, and the two photon ionization efficiency is enhanced because the photon energy is near resonant for the indole moiety in tryptophan. The peptides undergo a uniform deflection in the electric field. The deflection is proportional to the electric susceptibility, and the Langevin–Debye equation can be used to relate the electric susceptibility,  $\chi$ , to the permanent dipole moment,  $\mu$ :

$$\chi = \alpha + \frac{\langle \mu^2 \rangle_{T, F=0}}{3k_B T} \quad (1)$$

where  $\alpha$  is the polarizability and  $k_B$  is the Boltzmann constant. This approach is valid in the low field limit for a canonical ensemble, and where the molecules do not retain a memory of the orientation of their rotational motion as they travel through the field.

For neutral  $\text{AcWA}_n\text{NH}_2$  ( $W = \text{tryptophan}$ ,  $\text{NH}_2 = \text{amidated}$ ) peptides with  $n = 13$  and  $15$ , the measured dipole moments were consistent with  $\beta$ -sheet structures.<sup>76</sup> This result is consistent with Monte Carlo simulations performed for  $\text{AcWA}_{13}\text{NH}_2$  with a parallel tempering algorithm. Parallel tempering allows one to explore the energy landscape and determine free energies as a function of temperature. At 100 K, the helix is the lowest free energy structure for  $\text{AcWA}_{13}\text{NH}_2$ . However, at 300 K, the  $\beta$ -sheet and globular conformations have the lowest free energies. Examples of the  $\beta$ -sheet conformations found in the simulations are shown in Fig. 5. U-shaped  $\beta$ -hairpins and S-shaped conformations with two  $\beta$ -turns coexist, and it is the larger configurational entropy of the  $\beta$ -sheet conformations that leads them to have a lower free

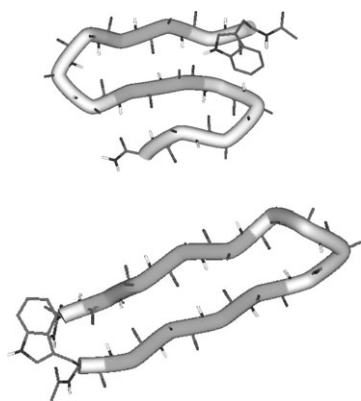


**Fig. 5** Examples of the  $\beta$ -structures found in the parallel tempering Monte Carlo simulations for  $\text{AcWA}_{13}\text{NH}_2$ . (From ref. 76. © American Chemical Society 2005).

energy than the helix at room temperature. Thus, it appears that the charge plays a critical role in determining the room temperature conformation: the  $\beta$ -sheet structures are favored for neutral peptides by configurational entropy but destroyed by a charge, while the helical conformation is stabilized by a charge. We were not able to observe helical structures for neutral peptides, despite considerable effort examining a variety of peptides. This indicates that the charge plays a critical role in stabilizing isolated helices.

### Helix propensities in unsolvated peptides

The helix propensity measures the tendency of a particular amino acid to make a helix. In aqueous solution, alanine has the highest helix propensity while glycine has the lowest. The difference between these two amino acids is small: glycine has no side chain, while alanine has a methyl group. In the gas phase we found that both  $\text{AcKG}_n + \text{H}^+$  and  $\text{AcG}_n\text{K} + \text{H}^+$  ( $G = \text{glycine}$ ) peptides adopt globular conformations.<sup>77</sup> In solution, the low helix propensity of glycine is usually attributed to its large conformational freedom, which makes the non-helical state favored entropically.<sup>78</sup> However, in the gas phase, the energies of the helical and globular conformations are probably more important. In the MD simulations, the glycine globules appear to be more stable than their alanine analogs, they have a lower strain energy and are able to twist upon themselves and form a greater number of well-aligned hydrogen bonds.

For amino acids with side chains (*i.e.* all of the natural amino acids except glycine), the helix propensities found in solution can be rationalized by side chain entropy (the entropy change due to the side chains that occurs when the amino acids are locked into a helical conformation).<sup>79,80</sup> Thus, valine, which has a bulky isopropyl side chain,  $\text{R} = -\text{CH}(\text{CH}_3)_2$ , has a low helix propensity (only slightly larger than glycine), while leucine, where the isopropyl group is offset by a methylene,  $\text{R} = -\text{CH}_2\text{CH}(\text{CH}_3)_2$ , has a high helix propensity (only slightly less than alanine). The helix propensities in the gas phase were obtained by examining the extent of helix formation in a variety of designed peptides. For example, the high helix propensity of valine in the gas phase is indicated by the fact that  $\text{AcKV}_n + \text{H}^+$  peptides (where the lysine is at the wrong end to promote helix formation) are helical for  $n > 13$  (while the leucine and alanine analogs,  $\text{AcKL}_n + \text{H}^+$  and  $\text{AcKA}_n + \text{H}^+$ , are globular). From these studies it appears that the helix propensities for the non-polar aliphatic amino acids in the gas phase are  $\text{V} > \text{L} > \text{A} \gg \text{G}$  (compared with  $\text{A} > \text{L} \gg \text{V} > \text{G}$  in solution).<sup>81,82</sup> The ordering of the helix propensities found in the absence of a solvent ( $\text{V} > \text{L} > \text{A} \gg \text{G}$ ) appear to reflect the stability of the non-helical, globular conformation. Peptides consisting of amino acids with large non-polar side chains make less compact and higher energy globules, so that the helical conformation is favored.

### Tuning the energies of helices and globules

Glycine has a low helix propensity, so incorporating glycine into alanine peptides destabilizes the helical conformation relative to the globule. A remarkably large number of glycine residues are required to disrupt helix formation.<sup>83</sup> For

example,  $\text{AcA}_5\text{G}_3\text{A}_5\text{K} + \text{H}^+$  and  $\text{AcA}_6\text{G}_5\text{A}_6\text{K} + \text{H}^+$  are both almost 100% helical at room temperature, while  $\text{AcA}_2\text{G}_9\text{A}_2 + \text{H}^+$  is almost 100% globular. The number of glycines and alanines in a peptide can be adjusted so that the relative stabilities of the helical and globular conformations are very similar.  $\text{AcA}_4\text{G}_7\text{A}_4$  is an example.<sup>84</sup> Four distinct conformations are observed for this peptide at low temperature, indicating that its energy landscape is broad and flat. As the temperature is raised above 230 K, some of the conformations begin to interconvert and disappear, and above 280 K only a single narrow peak (at a drift time close to that expected for the globule) remains. As the temperature is raised to 400 K, the peak gradually shifts to the position expected for the helix. The peak remains narrow as it shifts, which indicates that interconversion between the helix and globule is much faster than the timescale of the drift time measurements. Thus, the transition from globule to helix occurs under thermodynamic control. The peptide becomes more helical as the temperature is raised, and so the helix must be favored over the globule entropically. The globule is expected to have a higher configurational entropy than the helix, and so for the entropy of the helix to exceed that of the globule, the helix must have a higher vibrational entropy. This could result from the helix having low frequency longitudinal modes for which there are no counterparts in the globule.<sup>85</sup>

Context also appears to influence the stability of unsolvated helices.<sup>86</sup> Context deals with how amino acids interact with their neighbors. In an  $\alpha$ -helix, the  $i$  and  $i + 4$  residues can interact with each other. Two incompatible amino acids may destabilize the helix, while two compatible ones may promote helix formation.  $\text{AcA}_4\text{G}_7\text{A}_4 + \text{H}^+$  (discussed above) and  $\text{Ac}(\text{AG})_7\text{A} + \text{H}^+$  both have the same composition, but they have different sequences, and  $\text{Ac}(\text{AG})_7\text{A} + \text{H}^+$  is substantially less helical than  $\text{AcA}_4\text{G}_7\text{A}_4 + \text{H}^+$  at 400 K. This difference probably results because the  $\text{Ac}(\text{AG})_7\text{A} + \text{H}^+$  is more flexible and able to generate a lower energy globule. Studies of helix formation in a series of  $\text{Ac}[\text{G12A3}]\text{K} + \text{H}^+$  peptides show that the highest helix abundance occurs when alanine residues are grouped together in center (*i.e.*,  $\text{AcG}_6\text{A}_3\text{G}_6\text{K} + \text{H}^+$ ) and the lowest helix abundance occurs when the alanines are distributed throughout the peptide (*i.e.*,  $\text{AcG}_3\text{AG}_5\text{AG}_4\text{AK} + \text{H}^+$ ).

### $\alpha$ -helix or $\pi$ -helix preference in unsolvated peptides

The  $\alpha$ -helix is by far the most common helix found in proteins. The more-tightly wrapped  $3_{10}$ -helix with  $i, i + 3$  hydrogen bonds (compared to  $i, i + 4$  in the  $\alpha$ -helix) also occurs frequently. On the other hand, the more loosely wrapped  $\pi$ -helix (with  $i, i + 5$  hydrogen bonds) is rare.<sup>87–89</sup> There have been several reports of  $\pi$ -helical conformations in molecular dynamics simulations of peptides,<sup>90–94</sup> though Feig *et al.* suggest that these are the result of force field artifacts.<sup>95</sup> The measured cross sections for unsolvated alanine peptide ions (*i.e.*  $\text{AcA}_n\text{K} + \text{H}^+$ ) indicate that they prefer an  $\alpha$ -helical conformation. However, when glycines are incorporated into the peptides, the situation is less clear cut. In the simulations for  $\text{AcA}_4\text{G}_7\text{A}_4 + \text{H}^+$  both  $\alpha$ -helices and partial  $\pi$ -helices were observed, and the measured cross sections show features

**Table 1** Percent helix content determined from the ion mobility measurements at 213 K

Peptide name	Peptide sequence	E K interaction	Percent helix at 213 K
3A12G	AcAAAGGGGGGGGGGGGK	None	30
E7K11	AcAAAGGGEGGGKGGGGK	$i, i + 4$	12
E7K12	AcAAAGGGEGGGKGGGGK	$i, i + 5$	24
E7K13	AcAAAGGGEGGGKGGGK	$i, i + 6$	0

consistent with both.<sup>84</sup> To resolve this issue we designed a series of peptides incorporating glutamic acid (E) and lysine at specific locations. In solution, E and K residues positioned at  $i, i + 4$  are known to stabilize an  $\alpha$ -helix by forming a hydrogen bonded ion pair.<sup>46,96–100</sup> It is not clear that the charges on the EK ion pair will remain separated in the absence of the solvent. However, neutral E and K may still interact, though less strongly, through hydrogen bonds. E and K in the  $i, i + 4$  positions,  $\text{AcAAAGGGEGGGKGGGGK}$  (E7K11), should be stabilizing for both an  $\alpha$ -helix and a  $\pi$ -helix.

For  $i, i + 5$ ,  $\text{AcAAAGGGEGGGKGGGGK}$  (E7K12), the E and K are on opposite faces of an  $\alpha$ -helix (*i.e.* destabilizing) but on the same face of a  $\pi$ -helix (*i.e.* stabilizing). While  $i, i + 6$ ,  $\text{AcAAAGGGEGGGKGGGK}$  (E7K13), is destabilizing for both an  $\alpha$ -helix and a  $\pi$ -helix. Table 1 shows the percent helical content determined from the drift time distributions for the three peptides mentioned above and  $\text{AcAAAGGGGGGGGGGGGK}$  (3A12G), which lacks an E and K pair.

Of the three peptides with EK residues, E7K12 has the highest percent helix. This indicates that these peptides show a higher propensity to form  $\pi$ -helices than  $\alpha$ -helices. Since polyalanine based peptides are  $\alpha$ -helical, the preference for a  $\pi$ -helical arrangement is residue dependent. The 3A12G peptide in Table 1 that lacks an EK pair has the highest percent helix. Apparently, the incorporation of residues that can form hydrogen bonds decreases the stability of the helical state in the gas phase, presumably because the side chain competes for the backbone hydrogen bonding sites. This is a general result: incorporating residues capable of hydrogen bond formation destabilizes the unsolvated helices.

### Conformational changes and melting

$\text{AcA}_{15}\text{K} + \text{H}^+$  helices survive up to 725 K before dissociating. However, when the helices are destabilized by incorporating glycine residues, conformational changes can occur at a much lower temperature. For example, transitions between helical and globular conformations for  $\text{Ac}(\text{AGG})_5\text{K} + \text{H}^+$  occur at just below room temperature. It is only in the last decade that the kinetics of helix folding and unfolding transitions have been examined for short peptides in aqueous solution.<sup>101–104</sup> Fig. 6 shows drift time distributions recorded for  $\text{Ac}(\text{AGG})_5\text{K} + \text{H}^+$  at temperatures between 223 K and 295 K. At low temperature, there are two well-resolved peaks. As the temperature is raised a bridge forms between the two peaks that results from the helix (longer drift time) converting into the globule (shorter drift time) as the ions travel through the drift tube. As the temperature is raised the peak due to the helix

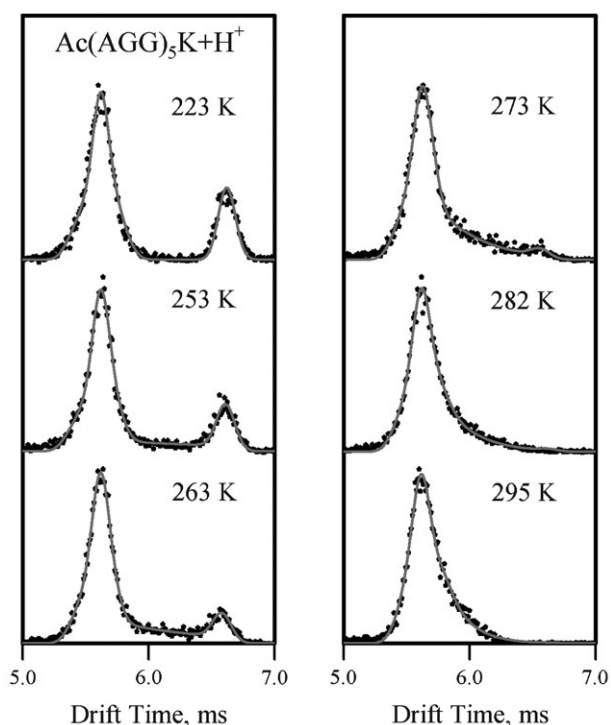


**Fig. 6** Drift time distributions for  $\text{Ac(AGG)}_5\text{K} + \text{H}^+$  as a function of temperature. The points are the experimental results, and the lines are simulations performed to determine rate constants. (From ref. 28. © American Chemical Society 2001).

disappears. The changes in the drift times in Fig. 6 occur because as the temperature is raised the rate at which the helix converts into the globule increases. The lines in Fig. 6 are the result of simulations performed to determine rate constants for the conversion of the helix into the globule. The rate constant increases from around  $2.1 \times 10^4 \text{ s}^{-1}$  at 253 K to around  $5.5 \times 10^6 \text{ s}^{-1}$  at 282 K. An Arrhenius plot ( $\ln k$  against  $1/T$ ) yields an activation energy of  $42.9 \text{ kJ mol}^{-1}$  for unfolding the  $\text{Ac(AGG)}_5\text{K} + \text{H}^+$  helix. As the number of AGG units in the peptide is increased the amount of helix present at low temperatures decreases, and for  $\text{Ac(AGG)}_8\text{K} + \text{H}^+$  the helix has essentially vanished.<sup>105</sup> On the other hand, the activation energies for helix unfolding increase as the number of AGG units increase, from  $42.9 \text{ kJ mol}^{-1}$  for  $\text{Ac(AGG)}_5\text{K} + \text{H}^+$  to  $61.3 \text{ kJ mol}^{-1}$  for  $\text{Ac(AGG)}_7\text{K} + \text{H}^+$ . This increase suggests that unfolding occurs through a concerted process involving the whole peptide, rather than by fraying from the ends of the helix. The lowest energy structure found in the MD simulations for  $\text{Ac(AGG)}_5\text{K} + \text{H}^+$  peptide is the partially helical conformation shown in Fig. 7.<sup>28,45</sup> This conformation appears to result from a partial untwisting of the helix and it is unusual because it has backward pointing hydrogen bonds (*i.e.* hydrogen bonds that point in the opposite direction to the others in the helix). The backward pointing hydrogen bonds are stabilized by electrostatic interactions with the helix dipole, and they can occur here because of the conformational flexibility of glycine. Some of the  $\text{Ac(AGG)}_5\text{K} + \text{H}^+$  MD simulations starting from an  $\alpha$ -helix unravel into the partially helical conformation shown in Fig. 7, but further unraveling into a

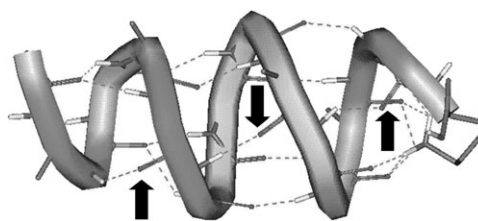


**Fig. 7** Snapshot of the lowest energy conformation found in the MD simulations of the  $\text{Ac(AGG)}_5\text{K} + \text{H}^+$  peptide. The arrows show the backward pointing hydrogen bonds. (From ref. 28. © American Chemical Society 2001).

globule was not observed to occur on the timescale of the simulations. This suggests that there may be an activation barrier to further untwisting. A concerted untwisting process could account for the increase in the measured activation energy with the number of AGG units.

Intramolecular proton transfer can also induce conformational changes.<sup>106</sup> The peptide  $\text{RA}_{15}\text{K}$  ( $\text{R} = \text{arginine}$ ) has basic residues at both the N- and C-termini. If the proton is sequestered at the C-terminus, this peptide should form a helix; while if it is protonated at the N-terminus, a globule should result. The gas phase basicity of the guanidinium group of arginine is around  $70 \text{ kJ mol}^{-1}$  larger than the  $\epsilon$ -amino group of lysine, so for a helix to form the process must be sufficiently exothermic to compensate for protonation at the less favorable site. Fig. 8 shows a plot of the cross sections determined for  $\text{RA}_{15}\text{K}$  as a function of temperature. At room temperature, both a helix and globule are observed, but as the temperature is raised to around 350 K the globule converts into the helix. This behavior indicates that the helix is lower in energy than the globule.

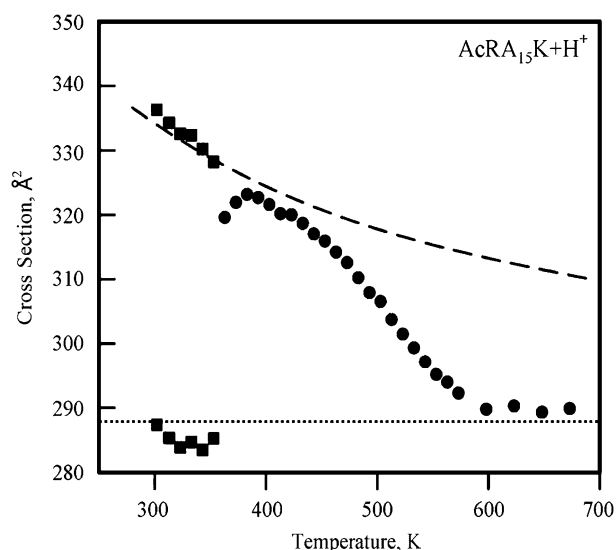


**Fig. 8** Cross sections recorded for  $\text{AcRA}_{15}\text{K} + \text{H}^+$  as a function of temperature. The squares represent cross sections determined from the center of the peaks (where there are clearly two resolved peaks) while the circles are obtained by averaging over the distribution (when the two peaks have merged). The dashed line shows the expected temperature dependence of the cross sections for a rigid helix. The dotted line is a guide. (From ref. 106. © American Chemical Society 2006).

The dashed line in Fig. 8 was obtained by taking the lowest energy helical conformation found in the room temperature MD simulations and calculating its cross section as a function of temperature. The measured cross sections start to depart significantly from this line for temperatures above 450 K. Above 600 K, the cross sections level off at a value only slightly larger than the room temperature cross section for the globule. In Fig. 3, the measured cross sections for the AcKA<sub>15</sub> + H<sup>+</sup> globule are almost independent of temperature. Thus, the RA<sub>15</sub>K points above 600 K are attributed to a globule. Since the cross sections for a rigid globule decrease with increasing temperature (see Fig. 3) cross sections that are independent of temperature indicate that the globule expands as the temperature is raised. As the globule expands, more conformations become accessible, and the entropy of the globule increases. For the RA<sub>15</sub>K peptide, this increase in the entropy presumably leads to the globule becoming the lowest free energy structure as the temperature is raised.

### Hydration of unsolvated peptides

The ability to generate unsolvated peptides raises the possibility of exposing them to water and studying hydration, one water molecule at a time.<sup>107–113</sup> Hydration studies were performed by admitting a known partial pressure of water vapor into the drift tube, and determining the amount of peptide that adsorbs water under equilibrium conditions. Fig. 9 which shows mass spectra recorded for globular AcKA<sub>20</sub> + H<sup>+</sup> and helical AcA<sub>20</sub>K + H<sup>+</sup> after exposure to 5.9 mtorr of water vapor at 224 K.<sup>112</sup> The low temperature is required to

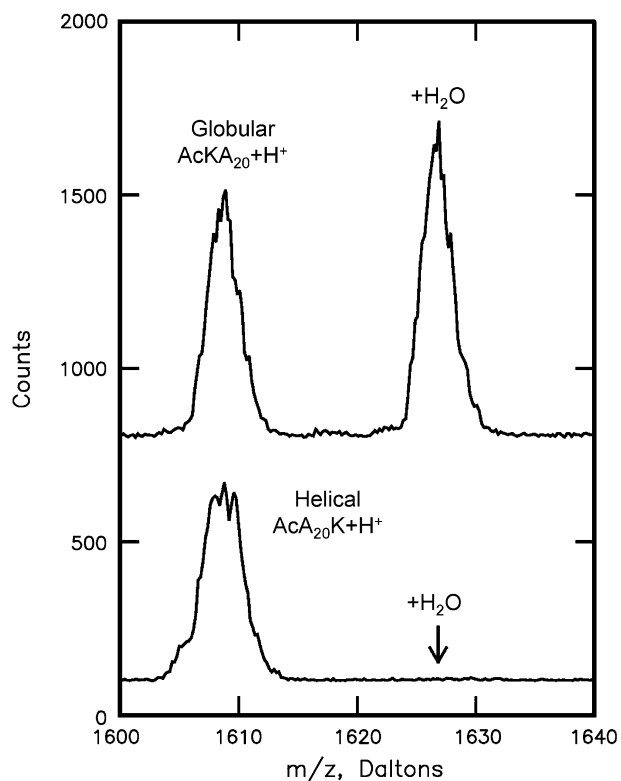


**Fig. 9** Mass spectra for AcKA<sub>20</sub> + H<sup>+</sup> (top) and AcA<sub>20</sub>K + H<sup>+</sup> (bottom) when exposed to 5.9 mtorr of water vapor at 224 K. (From ref. 112. © American Chemical Society 2002).

get the water to stick: at room temperature water does not stick to either peptide. Even at 224 K, water only sticks to the globular conformation. Thus, the globule adsorbs water much more strongly than the helix. At first glance, it might be thought that the most favorable binding site for the water would be near the site of protonation. However, MD simulations indicate that this is not a favorable binding site.<sup>110–112</sup> The protonation site is involved in several strong intramolecular hydrogen bonds to the peptide, and in order to bind the water, one or more of these hydrogen bonds must be disrupted. The criteria for a strong water binding site is to maximize the number of new hydrogen bonds formed between the water and the peptide, while minimizing the disruption of existing intramolecular hydrogen bonds. The most favorable binding sites for a water molecule appear to be clefts or pockets on the peptide surface that the water can enter and establish a network of hydrogen bonds. These sites are available on the globular conformation, but lacking on the helix. If a water molecule is placed near the middle of the helix it either desorbs or migrates to one of the ends where hydrogen bonding partners are available. The C-terminus appears to be the most favorable binding site, because the charge provides some additional electrostatic stabilization. Even though the charge site is less well shielded than in the globule, this is still not a strong binding site, and the water binding energy remains significantly below that found for the globule, where a network of hydrogen bonds can be established.

The fact that water adsorbs much less strongly on helices than globules provides a way to distinguish between these two conformations for small peptides, where ion mobility measurements are ambiguous because the helix and globule have similar average cross sections. From studies of the propensity to adsorb water onto AcA<sub>n</sub>K + H<sup>+</sup> and AcKA<sub>n</sub> + H<sup>+</sup> with  $n = 4–10$ , it was concluded the  $n = 8$  is the smallest AcA<sub>n</sub>K + H<sup>+</sup> peptide to show a significant helical content.<sup>114</sup> Water adsorption measurements on AcV<sub>n</sub>K + H<sup>+</sup> and AcL<sub>n</sub>K + H<sup>+</sup> with  $n = 5–10$  suggest that the helix emerges at  $n = 8$  for these peptides as well.

### Non-covalent interactions between unsolvated peptides

Weak non-covalent interactions are responsible for the organization of secondary structure elements into tertiary structure domains. Complex formation between unsolvated helical peptides can provide information on the intrinsic intramolecular interactions between helices in the absence of a solvent. The head-to-toe helical complex of two AcKA<sub>15</sub> + H<sup>+</sup> peptides, shown in Fig. 1(b), was mentioned above. In this complex, the helical conformation is stabilized by the protonated lysine side chain from one peptide interacting with the C-terminus of the other. The AcKA<sub>15</sub> + H<sup>+</sup> monomer is globular, and the dimer represents an interesting example of the local environment changing the secondary structure. Dimers are also observed for peptides that have helical monomers. For example, the complex formed between Ac(GA)<sub>7</sub>K + H<sup>+</sup> and AcA(GA)<sub>7</sub>K + H<sup>+</sup> has a cross section that is consistent with the V-shaped geometry shown in Fig. 10(a).<sup>115–117</sup> Here, the helical peptides are linked by an “exchanged lysine” motif where the lysine from one peptide interacts with the C-terminus

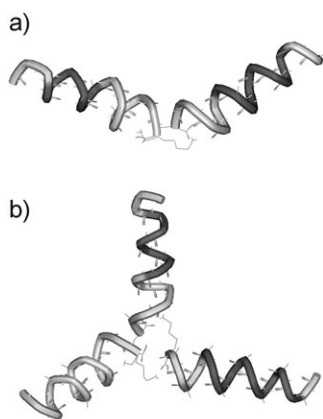


**Fig. 10** Conformations of (a) a helical dimer; and (b) a helical trimer assembled from  $\text{Ac}(\text{GA})_7\text{K} + \text{H}^+$  and  $\text{AcA}(\text{GA})_7\text{K} + \text{H}^+$ . (From ref. 115. © American Chemical Society 2002).

of the other. This is a common binding motif; the pinwheel-shaped helical trimer, shown in Fig. 10(b), has a similar exchanged lysine arrangement holding the helices together. The calculated cross sections for the pinwheel geometry match the measured values for the trimer. The trimer is the largest complex that has been observed for these peptides. The V-shaped arrangement in Fig. 10(a) is preferred over the “coiled-coil” arrangement with side-by-side helices because, in the parallel coiled-coil arrangement, the helix dipoles are parallel, which leads to unfavorable electrostatic interactions. The pin-wheel shaped geometry minimizes these unfavorable interactions for the trimer.

When the helices are arranged in an antiparallel arrangement (so that the interaction between the helix dipoles is favorable) an antiparallel coiled-coil geometry results.<sup>118,119</sup> For example, the peptide  $\text{AcA}_{14}\text{KG}_3\text{A}_{14}\text{K} + 2\text{H}^+$  has a helix-turn-helix motif with two  $\text{A}_{14}\text{K}$  helical units linked together by a short  $\text{G}_3$  loop. Fig. 11 shows cross sections recorded for  $\text{AcA}_{14}\text{KG}_3\text{A}_{14}\text{K} + 2\text{H}^+$  as a function of temperature. At low temperature, three conformations are observed, which are assigned to the coiled-coil geometry, shown in Fig. 11(a), an

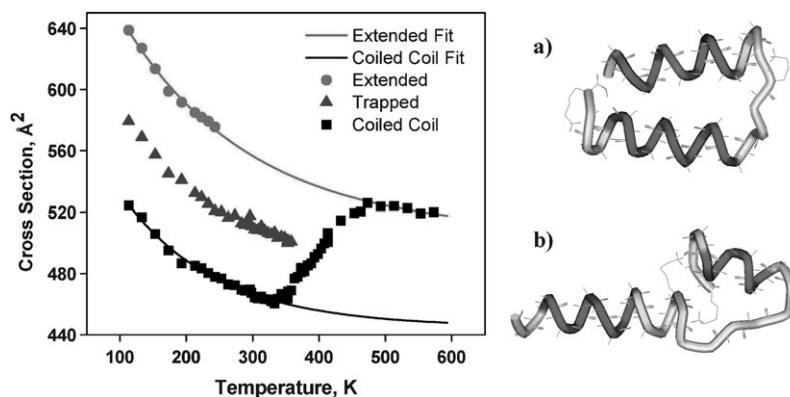


**Fig. 11** Cross sections recorded for  $\text{AcA}_{14}\text{KG}_3\text{A}_{14}\text{K} + 2\text{H}^+$  as a function of temperature. The circular points are assigned to the extended or uncoupled conformation. The triangular points are assigned to the high energy trapped conformation, and the square points at temperatures less than 330 K are assigned to the coiled-coil geometry where the helices are aligned. The lines show the extrapolated values for the extended conformation (upper line) and the coiled-coil geometry (lower line). The conformations on the left show snapshots from MD simulations. (a) is the coiled-coil geometry and (b) is the trapped geometry. (From ref. 118 and 119. © American Chemical Society 2003).

**Table 2** Enthalpy and entropy changes for helix uncoupling reactions in unsolvated peptides with a helix-turn-helix motif

Peptide	$\Delta H^\circ/\text{kJ mol}^{-1}$	$\Delta S^\circ/\text{J K}^{-1} \text{mol}^{-1}$
G3: $\text{AcA}_{14}\text{KG}_3\text{A}_{14}\text{K} + 2\text{H}^+$	$-49 \pm 2$	$124 \pm 4$
Sar3: $\text{AcA}_{14}\text{KSar}_5\text{A}_{14}\text{K} + 2\text{H}^+$	$-43 \pm 3$	$93 \pm 7$
G7: $\text{AcA}_{14}\text{KG}_7\text{A}_{14}\text{K} + 2\text{H}^+$	$-56 \pm 2$	$158 \pm 4$

extended or uncoupled geometry where the helices are not coupled together in a coiled-coil, and a high energy metastable structure assigned to the geometry shown in Fig. 11(b). At low temperature, all three conformations are observed, but as the temperature is raised they all anneal into the coiled-coil geometry (see Fig. 11). However, as the temperature is raised further, the helices become uncoupled. This occurs over a temperature range of 360–410 K. Within this temperature range, the peak in the drift time distributions remains narrow and shifts gradually from the position expected for the coiled-coil to the position expected for the extended or open structure. This behavior is characteristic of a change occurring under equilibrium control, where the transition between the two conformations is fast on the timescale of the drift time measurements. The value of the measured cross section relative to the values of the cross sections for the coiled-coil and extended conformation provides a measure of the time spent in each conformation, which is related to the equilibrium constant. A Van’t Hoff plot of  $\ln K$  against  $1/T$  yields the enthalpy change ( $\Delta H^\circ = -49 \pm 2 \text{ kJ mol}^{-1}$ ) and entropy change ( $\Delta S^\circ = 124 \pm 4 \text{ J K}^{-1} \text{mol}^{-1}$ ) for the helix coupling  $\rightleftharpoons$  uncoupling equilibrium.  $\Delta H^\circ$  is the enthalpy change for uncoupling the two helices, the value of  $49 \text{ kJ mol}^{-1}$  found here is mainly due to electrostatic and van der Waals interactions, because there are no specific chemical interactions binding the helices together in this peptide.  $\Delta S^\circ$  is essentially the entropy change for freeing up the glycine loop. The backbone entropy of glycine has previously been estimated to be around  $28 \text{ J K}^{-1} \text{mol}^{-1}$ ,<sup>120</sup> and  $3 \times 28 = 84 \text{ J K}^{-1} \text{mol}^{-1}$ , which is close to the measured entropy change ( $114 \text{ J K}^{-1} \text{mol}^{-1}$ ). Similar measurements were performed for several other peptides with a helix-turn-helix motif, examples are

shown in Table 2. In the Sar3 peptide, the G<sub>3</sub> loop is replaced by a loop of three sarcosines. Sarcosine is an isomer of alanine where the methyl group is located on the amide nitrogen instead of the  $\alpha$ -carbon. As a consequence, sarcosine cannot form a helical hydrogen bond through the amide nitrogen. The entropy change with a Sar3 loop is significantly lower than with G3 because the methyl group restricts the conformational space accessible with the Sar3 loop. With a G7 loop the entropy change increases substantially, but the change is much less than four times the backbone entropy of glycine ( $4 \times 28 = 112 \text{ J K}^{-1} \text{ mol}^{-1}$ ), because as the loop gets longer, it gets floppier, and a smaller entropy change is expected.

## Conclusions

Some of the factors that stabilize unsolvated helices and sheets have been identified. Extended  $\beta$ -sheet structures are stable for neutral peptides *in vacuo*, but they are disrupted by a charge. On the other hand, charge plays a critical role in stabilizing the helical conformation, and helices have not been observed for neutral peptides. Two main conformations were found for charged peptides: a helix and globule. In many cases, the factors that stabilize unsolvated helices are different from the factors that stabilize them in solution. For example, in the absence of a solvent, incorporating hydrogen bonding residues in stabilizing positions destabilizes the helix relative to the globule. Thus, the most stable unsolvated helices are made from non-polar amino acids. Charge-stabilized, polyalanine based peptides remain 100% helical to over 400 °C. Polyalanine based helices can be destabilized by incorporating glycine. By adjusting the number of glycine and alanine residues, the stability of the helical and globular conformations can be balanced so that conformational changes occur at close to room temperature. As the temperature is raised, protons no longer remain sequestered at the most basic site, but can become mobile, hopping along the backbone amide groups. This intramolecular proton transfer can also cause conformational changes.

Water has a low affinity for unsolvated peptides, even charged peptides, and it is necessary to cool the system to quite low temperature before a water molecule will stick. The most favorable binding sites are pockets or clefts where the water can establish a network of hydrogen bonds, while causing the minimum disruption to the existing intramolecular hydrogen bonding network. The hydration properties depend on the conformation: globules adsorb water molecules much more strongly than helices, because helices lack favorable binding sites.

The ability to design peptides that form stable helices in the absence of a solvent permits studies of the interactions between unsolvated helices. The formation of complexes between helical peptides is one avenue that was explored. The geometries of these complexes are strongly influenced by interactions between the helix dipoles. Thus, a parallel coiled-coil (side by side) arrangement of helices is unfavorable, and helices linked together head-to-head tend to repel each other (leading to V-shaped or pinwheel-shaped geometries). On the other hand, the anti-parallel side-by-side arrangement has favorable interactions between the helix dipoles. Peptides with a designed helix-turn-

helix motif form a coiled-coil geometry at low temperature, while the helices become uncoupled as the temperature is raised.

The results described above provide a first glimpse at the properties of unsolvated peptides large enough to generate secondary structure. The goal now should be to develop more quantitative measures that can provide a thermodynamic scale for important intramolecular interactions in the absence of a solvent. One target should be to develop a thermodynamic scale of the helix propensities in the absence of a solvent. The helix-turn-helix motif described above provides an opportunity to determine thermodynamic information about specific interactions between helices. Ultimately, these studies will help to understand the structures of proteins and protein assemblies both in solution and in environments where the solvent is excluded, such as the inside of membranes.

## Acknowledgements

This work described in this article was supported by the National Institutes of Health (R01 GM58141). I am grateful to the many coworkers and collaborators that contributed to the research described here.

## References

- 1 K. A. Dill, *Biochemistry*, 1990, **29**, 7133–7155.
- 2 S. K. Chowdhury, V. Katta and B. T. Chait, *J. Am. Chem. Soc.*, 1990, **112**, 9012–9013.
- 3 R. R. Hudgins, J. Woienckhaus and M. F. Jarrold, *Int. J. Mass Spectrom. Ion Processes*, 1997, **165/166**, 497–507.
- 4 A. A. Rostom and C. V. Robinson, *J. Am. Chem. Soc.*, 1999, **121**, 4718–4719.
- 5 J. L. Fye, J. Woienckhaus and M. F. Jarrold, *J. Am. Chem. Soc.*, 1998, **120**, 1327–1328.
- 6 Y. Mao, M. A. Ratner and M. F. Jarrold, *J. Am. Chem. Soc.*, 2000, **122**, 2950–2951.
- 7 E. Wallin and G. von Hiejne, *Protein Sci.*, 1998, **7**, 1029–1038.
- 8 A special issue of Physical Chemistry Chemical Physics is dedicated to Bioactive Molecules in the Gas Phase, *Phys. Chem. Chem. Phys.* 2004, **6**, issue 10.
- 9 E. G. Robertson and J. P. Simons, *Phys. Chem. Chem. Phys.*, 2001, **3**, 1–18.
- 10 T. S. Zwier, *J. Phys. Chem.*, 2001, **105**, 8827–8839.
- 11 T. V. Nguyen and D. W. Pratt, *J. Chem. Phys.*, 2006, **124**, 054317.
- 12 S. L. Koeniger, S. I. Merenbloom and D. E. Clemmer, *J. Phys. Chem. B*, 2006, **110**, 7017–7021.
- 13 A. E. Counterman and D. E. Clemmer, *J. Phys. Chem. B*, 2004, **108**, 4885–4898.
- 14 C. A. S. Barnes and D. E. Clemmer, *J. Phys. Chem. A*, 2003, **107**, 10566–10579.
- 15 A. T. Iavarone, J. Meinen and S. Schulze. J. H. Parks, *Int. J. Mass Spectrom.*, 2006, **253**, 172–180.
- 16 A. T. Iavarone and J. H. Parks, *J. Am. Chem. Soc.*, 2005, **127**, 8606–8607.
- 17 J. Gidden, E. S. Baker, A. Ferzoco and M. T. Bowers, *Int. J. Mass Spectrom.*, 2005, **240**, 183–193.
- 18 P. E. Barran, N. C. Polfer, D. J. Campopiano, D. J. Clarke, P. R. Langridge-Smith, R. J. Langley, J. R. W. Govan, A. Maxwell, J. R. Dorin, R. P. Millar and M. T. Bowers, *Int. J. Mass Spectrom.*, 2005, **240**, 273–284.
- 19 M. F. Bush, R. J. Saykally and E. R. Williams, *Int. J. Mass Spectrom.*, 2006, **253**, 256–262.
- 20 A. S. Lemoff, C. C. Wu, M. F. Bush and E. R. Williams, *J. Phys. Chem. A*, 2006, **110**, 3662–3669.
- 21 S. J. Ye, R. M. Moision and P. B. Armentrout, *Int. J. Mass Spectrom.*, 2006, **253**, 288–304.

- 22 M. T. Rodgers and P. B. Armentrout, *Acc. Chem. Res.*, 2004, **37**, 989–998.
- 23 K. Breuker and F. W. McLafferty, *Angew. Chem., Int. Ed.*, 2005, **44**, 4911–4914.
- 24 H. A. Sawyer, J. T. Marini, E. G. Stone, B. T. Ruotolo, K. J. Gillig and D. H. Russell, *J. Am. Soc. Mass Spectrom.*, 2005, **16**, 893–905.
- 25 B. T. Ruotolo, K. Giles, I. Campuzano, A. M. Sandercock, R. H. Bateman and C. V. Robinson, *Science*, 2005, **310**, 1658–1661.
- 26 D. E. Clemmer and M. F. Jarrold, *J. Mass Spectrom.*, 1997, **32**, 577–592.
- 27 T. Wyttenbach and M. T. Bowers, *Top. Curr. Chem.*, 2003, **225**, 207–232.
- 28 B. S. Kinnear, M. R. Hartings and M. F. Jarrold, *J. Am. Chem. Soc.*, 2001, **123**, 5660–5667.
- 29 M. Kohtani, J. E. Schneider, T. C. Jones and M. F. Jarrold, *J. Am. Chem. Soc.*, 2004, **126**, 16981–16987.
- 30 E. A. Mason and E. W. McDaniel, *Transport Properties of Ions in Gases*, Wiley, New York, 1988.
- 31 MACSIMUS is available from: <http://www.icpf.cas.cz/jiri/macsimus/default.htm>.
- 32 MOBCAL is available from: <http://nano.chem.indiana.edu>.
- 33 A. A. Shvartsburg and M. F. Jarrold, *Chem. Phys. Lett.*, 1996, **261**, 86–91.
- 34 M. F. Mesleh, J. M. Hunter, A. A. Shvartsburg, G. C. Schatz and M. F. Jarrold, *J. Phys. Chem.*, 1996, **100**, 16082–16086.
- 35 R. R. Hudgins, M. A. Ratner and M. F. Jarrold, *J. Am. Chem. Soc.*, 1998, **120**, 12974–12975.
- 36 R. R. Hudgins and M. F. Jarrold, *J. Am. Chem. Soc.*, 1999, **121**, 3494–3501.
- 37 A. Chakrabarty and R. L. Baldwin, *Adv. Protein Chem.*, 1995, **46**, 141–176.
- 38 K. T. O’Neil and W. F. DeGrado, *Science*, 1990, **250**, 646–651.
- 39 P. C. Lyu, M. I. Liff, L. A. Marky and N. R. Kallenbach, *Science*, 1990, **250**, 669–673.
- 40 D. E. Blagdon and M. Goodman, *Biopolymers*, 1975, **14**, 241–245.
- 41 K. R. Shoemaker, P. S. Kim, E. J. York, J. M. Stewart and R. L. Baldwin, *Nature*, 1987, **326**, 563–567.
- 42 J. S. Richardson and D. C. Richardson, *Science*, 1988, **240**, 1648–1652.
- 43 L. G. Presta and G. D. Rose, *Science*, 1988, **240**, 1632–1641.
- 44 B. Forood, E. J. Feliciano and K. P. Nambiar, *Proc. Natl. Acad. Sci. USA*, 1993, **90**, 838–842.
- 45 M. Damsbo, B. S. Kinnear, M. R. Hartings, P. T. Ruhoff, M. F. Jarrold and M. A. Ratner, *Proc. Natl. Acad. Sci. USA*, 2004, **101**, 7215–7222.
- 46 S. Marqusee and R. L. Baldwin, *Proc. Natl. Acad. Sci. USA*, 1987, **84**, 8898–8902.
- 47 S. Marqusee, V. H. Robbins and R. L. Baldwin, *Proc. Natl. Acad. Sci. USA*, 1989, **86**, 5286–5290.
- 48 M. Kohtani, T. C. Jones, J. E. Schneider and M. F. Jarrold, *J. Am. Chem. Soc.*, 2004, **126**, 7420–7421.
- 49 Y. Okamoto and U. H. E. Hansmann, *J. Phys. Chem.*, 1995, **99**, 11276–11287.
- 50 N. A. Alves and U. H. E. Hansmann, *Phys. Rev. Lett.*, 2000, **84**, 1836–1839.
- 51 Y. Peng, U. H. E. Hansmann and N. A. Alves, *J. Chem. Phys.*, 2003, **118**, 2374–2380.
- 52 B. H. Zimm and J. K. Bragg, *J. Chem. Phys.*, 1959, **78**, 498–500.
- 53 S. Lifson and A. Roig, *J. Chem. Phys.*, 1960, **34**, 1963–1974.
- 54 C. A. Rohl, A. Chakrabarty and R. L. Baldwin, *Protein Sci.*, 1996, **5**, 2623–2637.
- 55 F. B. Sheinerman and C. L. Brooks, *J. Am. Chem. Soc.*, 1995, **117**, 10098–10103.
- 56 C. A. Rohl and A. J. Doig, *Protein Sci.*, 1996, **5**, 1687–1696.
- 57 V. Muñoz and L. Serrano, *Nat. Struct. Biol.*, 1994, **1**, 399–409.
- 58 E. Lacroix, A. R. Viguera and L. Serrano, *J. Mol. Biol.*, 1998, **284**, 173–191.
- 59 G. Breaux and M. F. Jarrold, *J. Am. Chem. Soc.*, 2003, **125**, 10740–10747.
- 60 C. F. Rodriguez, A. Cunje, T. Shoeb, I. K. Chu, A. C. Hopkinson and K. W. M. Siu, *J. Am. Chem. Soc.*, 2001, **123**, 3006–3012.
- 61 K. Zhang, C. J. Cassady and A. Chung-Phillips, *J. Am. Chem. Soc.*, 1994, **116**, 11512–11521.
- 62 B. Paizs, I. P. Csonka, G. Lendvai and S. Suhai, *Rapid Commun. Mass Spectrom.*, 2001, **15**, 637–650.
- 63 M. Kohtani, G. A. Breaux and M. F. Jarrold, *J. Am. Chem. Soc.*, 2004, **126**, 1206–1213.
- 64 R. R. Hudgins, Y. Mao, M. A. Ratner and M. F. Jarrold, *Biophys. J.*, 1999, **76**, 1591.
- 65 R. S. Johnson, S. A. Martin and K. Biemann, *Int. J. Mass Spectrom. Ion Processes*, 1988, **86**, 137–154.
- 66 O. Bulet, R. S. Orkiszewski, K. D. Ballard and S. J. Gaskell, *Rapid Commun. Mass Spectrom.*, 1992, **6**, 658–662.
- 67 A. R. Dongré, J. L. Jones, A. Somogyi and V. H. Wysocki, *J. Am. Chem. Soc.*, 1996, **118**, 8365–8374.
- 68 V. H. Wysocki, G. Tsapralis, L. L. Smith and L. A. Breci, *J. Mass Spectrom.*, 2000, **35**, 1399–1406.
- 69 A. Q. Li, C. Fenselau and I. A. Kaltashov, *Proteins: Struct. Funct. Genet.*, 1998, **33**(Supplement 2), 22–27.
- 70 B. T. Ruotolo, C. C. Tate and D. H. Russell, *J. Am. Soc. Mass Spectrom.*, 2004, **15**, 870–878.
- 71 I. Compagnon, F. C. Hagermeister, R. Antoine, D. Rayane, M. Broyer, Ph. Dugourd, R. R. Hudgins and M. F. Jarrold, *J. Am. Chem. Soc.*, 2001, **123**, 8440–8441.
- 72 R. Antoine, I. Compagnon, D. Rayane, M. Broyer, Ph. Dugourd, G. Breaux, F. C. Hagermeister, D. Pippen, R. R. Hudgins and M. F. Jarrold, *J. Am. Chem. Soc.*, 2002, **124**, 6737–6741.
- 73 R. Antoine, I. Compagnon, D. Rayane, M. Broyer, Ph. Dugourd, G. Breaux, F. C. Hagermeister, D. Pippen, R. R. Hudgins and M. F. Jarrold, *Eur. Phys. J. D*, 2002, **20**, 583–587.
- 74 I. Compagnon, F. C. Hagermeister, R. Antoine, D. Rayane, M. Broyer, Ph. Dugourd, R. R. Hudgins and M. F. Jarrold, *J. Am. Chem. Soc.*, 2001, **123**, 8440–8441.
- 75 R. Antoine, I. Compagnon, D. Rayane, M. Broyer, Ph. Dugourd, G. Breaux, F. C. Hagermeister, D. Pippen, R. R. Hudgins and M. F. Jarrold, *J. Am. Chem. Soc.*, 2002, **124**, 6737–6741.
- 76 Ph. Dugourd, R. Antoine, G. A. Breaux, M. Broyer and M. F. Jarrold, *J. Am. Chem. Soc.*, 2005, **127**, 4675–4679.
- 77 R. R. Hudgins and M. F. Jarrold, *J. Phys. Chem. B*, 2000, **104**, 2154–2158.
- 78 M. Go, N. Go and H. A. Scheraga, *J. Chem. Phys.*, 1970, **52**, 2060–2079.
- 79 T. P. Creamer and G. D. Rose, *Proc. Natl. Acad. Sci. USA*, 1992, **89**, 5937–5941.
- 80 L. Piela, G. Nemethy and H. A. Scheraga, *Biopolymers*, 1987, **26**, 1273–1286.
- 81 B. S. Kinnear, D. T. Kaleta, M. Kohtani, R. R. Hudgins and M. F. Jarrold, *J. Am. Chem. Soc.*, 2000, **122**, 9243–9256.
- 82 B. S. Kinnear and M. F. Jarrold, *J. Am. Chem. Soc.*, 2001, **123**, 7907–7908.
- 83 D. T. Kaleta and M. F. Jarrold, *J. Phys. Chem. B*, 2001, **105**, 4436–4440.
- 84 B. S. Kinnear, M. R. Hartings and M. F. Jarrold, *J. Am. Chem. Soc.*, 2002, **124**, 4422–4431.
- 85 B. Ma, C.-J. Tsai and R. Nussinov, *Biophys. J.*, 2000, **79**, 2739–2753.
- 86 M. R. Hartings, B. S. Kinnear and M. F. Jarrold, *J. Am. Chem. Soc.*, 2003, **125**, 3941–3947.
- 87 B. W. Low and R. B. Baybutt, *J. Am. Chem. Soc.*, 1952, **74**, 5806–5807.
- 88 M. N. Fodje and S. Al-Karadaghi, *Protein Eng.*, 2002, **15**, 353–358.
- 89 T. M. Weaver, *Protein Sci.*, 2000, **9**, 201–206.
- 90 K. Lee, D. R. Benson and K. Kuczera, *Biochemistry*, 2000, **39**, 13737–13747.
- 91 H. Kovacs, A. E. Mark, J. Johansson and W. F. van Gunsteren, *J. Mol. Biol.*, 1995, **247**, 808–822.
- 92 W. A. Shirley and C. L. Brooks III, *Proteins: Struct. Funct. Genet.*, 1997, **28**, 59–71.
- 93 N. Gibbs, R. B. Sessions, P. B. Williams and C. E. Dempsey, *Biophys. J.*, 1997, **72**, 2490–2495.
- 94 J.-P. Duneau, S. Crouzy, Y. Chapron and M. Genest, *Theor. Chem. Acc.*, 1999, **101**, 87–91.
- 95 M. Feig, A. D. MacKerell and C. L. Brooks, *J. Phys. Chem. B*, 2003, **107**, 2831–2836.
- 96 P. C. Lyu, P. J. Gans and N. R. Kallenbach, *J. Mol. Biol.*, 1992, **223**, 343–350.

- 97 J. M. Scholtz, H. Qian, V. H. Robbins and R. L. Baldwin, *Biochemistry*, 1993, **32**, 9668–9676.
- 98 B. M. P. Huyghues-Despointes and R. L. Baldwin, *Biochemistry*, 1997, **36**, 1965–1970.
- 99 Z. Shi, C. A. Olson, A. J. Bell and N. R. Kallenbach, *Biopolymers*, 2001, **60**, 366–380.
- 100 J. R. Litowski and R. S. Hodges, *J. Biol. Chem.*, 2002, **277**, 37272–37279.
- 101 S. Williams, T. P. Causgrove, R. Gilmanshin, K. S. Fang, R. H. Callender, W. H. Woodruff and R. B. Dyer, *Biochemistry*, 1996, **35**, 691–697.
- 102 I. K. Lednev, A. S. Karnoup, M. C. Sparrow and S. A. Asher, *J. Am. Chem. Soc.*, 1999, **121**, 8074–8086.
- 103 D. T. Clarke, A. J. Doig, B. J. Stapley and G. R. Jones, *Proc. Natl. Acad. Sci. USA*, 1999, **96**, 7232–7237.
- 104 P. A. Thompson, V. Muñoz, G. S. Jas, E. R. Henry, W. A. Eaton and J. Hofrichter, *J. Phys. Chem. B*, 2000, **104**, 378–389.
- 105 M. R. Hartings, M. A. Ratner and M. F. Jarrold (to be published).
- 106 M. Kohtani, T. C. Jones, R. Sudha and M. F. Jarrold, *J. Am. Chem. Soc.*, 2006, **128**, 7193–7197.
- 107 J. Woenckhaus, Y. Mao and M. F. Jarrold, *J. Phys. Chem. B*, 1997, **101**, 847–851.
- 108 J. Woenckhaus, R. R. Hudgins and M. F. Jarrold, *J. Am. Chem. Soc.*, 1997, **119**, 9586–9587.
- 109 J. L. Fye, J. Woenckhaus and M. F. Jarrold, *J. Am. Chem. Soc.*, 1998, **120**, 1327–1328.
- 110 Y. Mao, M. A. Ratner and M. F. Jarrold, *J. Am. Chem. Soc.*, 2000, **122**, 2950–2951.
- 111 Y. Mao, M. A. Ratner and M. F. Jarrold, *J. Am. Chem. Soc.*, 2001, **123**, 6503–6507.
- 112 M. Kohtani and M. F. Jarrold, *J. Am. Chem. Soc.*, 2002, **124**, 11148–11158.
- 113 M. Kohtani, G. A. Breaux and M. F. Jarrold, *J. Am. Chem. Soc.*, 2004, **126**, 1206–1213.
- 114 M. Kohtani and M. F. Jarrold, *J. Am. Chem. Soc.*, 2004, **126**, 8454–8458.
- 115 D. T. Kaleta and M. F. Jarrold, *J. Am. Chem. Soc.*, 2002, **124**, 1154–1155.
- 116 D. T. Kaleta and M. F. Jarrold, *J. Phys. Chem. A*, 2002, **106**, 9655–9664.
- 117 D. T. Kaleta and M. F. Jarrold, *J. Phys. Chem. B*, 2003, **107**, 14529–14536.
- 118 D. T. Kaleta and M. F. Jarrold, *J. Am. Chem. Soc.*, 2003, **125**, 7186–7187.
- 119 L. W. Zilch, M. Kohtani, R. Krishnan, D. T. Kaleta and M. F. Jarrold (to be published).
- 120 C. Zhang, J. L. Cornette and C. Delisi, *Protein Sci.*, 1997, **6**, 1057–1064.



Save valuable time searching for that elusive piece of vital chemical information.

Let us do it for you at the Library and Information Centre of the RSC.

We are your chemical information support, providing:

- Chemical enquiry helpdesk
- Remote access chemical information resources
- Speedy response
- Expert chemical information specialist staff

Tap into the foremost source of chemical knowledge in Europe and send your enquiries to

[library@rsc.org](mailto:library@rsc.org)

12120515

RSCPublishing

[www.rsc.org/library](http://www.rsc.org/library)